Assessment of interaction-strength interpolation formulas for gold and silver clusters

Sara Giarrusso, Paola Gori-Giorgi, Fabio Della Sala, and Eduardo Fabiano

Citation: The Journal of Chemical Physics **148**, 134106 (2018); doi: 10.1063/1.5022669
View online: https://doi.org/10.1063/1.5022669
View Table of Contents: http://aip.scitation.org/toc/jcp/148/13
Published by the American Institute of Physics

Assessment of interaction-strength interpolation formulas for gold and silver clusters

Sara Giarrusso,[1] Paola Gori-Giorgi,[1] Fabio Della Sala,[2,3] and Eduardo Fabiano[2,3]
[1]*Department of Theoretical Chemistry and Amsterdam Center for Multiscale Modeling, FEW, Vrije Universiteit, De Boelelaan 1083, 1081HV Amsterdam, The Netherlands*
[2]*Institute for Microelectronics and Microsystems (CNR-IMM), Via Monteroni, Campus Unisalento, 73100 Lecce, Italy*
[3]*Center for Biomolecular Nanotechnologies @UNILE, Istituto Italiano di Tecnologia, Via Barsanti, I-73010 Arnesano, Italy*

(Received 17 January 2018; accepted 14 March 2018; published online 2 April 2018)

The performance of functionals based on the idea of interpolating between the weak- and the strong-interaction limits the global adiabatic-connection integrand is carefully studied for the challenging case of noble-metal clusters. Different interpolation formulas are considered and various features of this approach are analyzed. It is found that these functionals, when used as a correlation correction to Hartree-Fock, are quite robust for the description of atomization energies, while performing less well for ionization potentials. Future directions that can be envisaged from this study and a previous one on main group chemistry are discussed. *Published by AIP Publishing.* https://doi.org/10.1063/1.5022669

I. INTRODUCTION AND THEORETICAL BACKGROUND

Noble metal clusters, in particular, those made of silver and gold, are of high interest for different areas of materials science and chemistry as well as for technological applications.[1–22] Noble metals clusters display, in fact, peculiar properties that differ from those of the bulk materials, due to the higher reactivity of the surface atoms. Moreover, these properties can be often tuned by varying the size and shape of the clusters.[2,10,13,15,23–28] For these reasons, the study of the electronic properties of metal clusters is currently a very active research field,[29–39] with many available experimental techniques.[40–47] Nonetheless, in most cases, information from theoretical calculations is fundamental to provide a better understanding of the results and to aid the correct interpretation of the experimental data.[29,30,39,48–52]

Computational studies of noble metal clusters are, however, not straightforward[53] because of the small single-particle energy gap, implying a possible multi-reference character of the electronic states, and due to the complex correlation effects characterizing such systems. For these reasons, in principle, an accurate description of the electronic structure can only be achieved by high-level correlated multi-reference approaches.[54,55] However, these methods are hardly applicable for the study of clusters, due to the very high computational cost. On the other hand, "conventional" single-reference wave-function methods [e.g., Møller-Plesset (MP) perturbation theory,[56,57] configuration interaction,[58,59] or coupled cluster[60,61]] often display important basis set and/or truncation errors, even for relatively small cluster sizes, which prevent the achievement of accurate, reliable results. Thus, one of the most used computational tools to study noble metal clusters is Kohn-Sham density-functional theory (DFT).[62–64]

DFT calculations on noble metal clusters are often performed using a semilocal approximation for the exchange-correlation (XC) functional, e.g., the generalized gradient approximation (GGA)[65] or the meta-GGAs.[66] This is an efficient approach,[25,26,33,35,37,38,48,49,67–69] but in various cases, it has also shown limited accuracy, especially in the not so rare case when it is necessary to discriminate between isomers with rather similar energies (for example, in the prediction of the two- to three-dimensional crossover in gold and silver clusters[38,50]). However, unlike in the case of main group molecular calculations, the use of hybrid functionals, which include a fraction of exact exchange, is not able to provide a systematic improvement. Instead, it often leads to a worsening of the results.[38,69] The origin of this problem possibly traces back to the too simplistic idea of mixing a fixed fraction of exact exchange with a semilocal approximation.

In the hybrid wavefunction-DFT formalism, a certain fraction a of the electron-electron interaction is treated within a wave function method, while the remaining energy is captured with a semilocal functional. In a compact notation,[70] this can be written as

$$E_0 = \min_{\Psi} \left\{ \langle \Psi | \hat{T} + a\,\hat{V}_{ee} + \hat{V}_{ne} | \Psi \rangle + \bar{E}^{a}_{\mathrm{Hxc}}[\rho_\Psi] \right\}, \qquad (1)$$

where the complementary Hartree-exchange-correlation functional $\bar{E}^{a}_{\mathrm{Hxc}}$ depends on Ψ only through its density ρ_Ψ. In Eq. (1), $\hat{T}$ is the electronic kinetic energy operator, $\hat{V}_{ee}$ is the electron-electron repulsion operator and $\hat{V}_{ne}$ is the external potential due to the nuclei. The standard hybrid and double-hybrid functionals of KS DFT can be seen as different approximations for the wavefunction Ψ appearing in Eq. (1): when the minimization over Ψ is restricted to single Slater determinants, we obtain the usual hybrid functional scheme, which mixes a fraction a of Hartree-Fock (HF) exchange with a semilocal

functional. If on top of that we use second-order perturbation theory, we obtain single-parameter double-hybrid functionals, as shown in Ref. 70.

The XC part $E_{xc}[\rho]$ of $\bar{E}^{a}_{\mathrm{Hxc}}$ that needs to be approximated in the standard hybrid functionals formalism is usually modeled starting from the adiabatic connection formula[71–74]

$$E_{xc}[\rho] = \int_0^1 W_\lambda[\rho] d\lambda, \tag{2}$$

where λ is the interaction strength and $W_\lambda[\rho] = \langle \Psi_\lambda[\rho] | \hat{V}_{ee} | \Psi_\lambda[\rho] \rangle - U[\rho]$ is the density-fixed linear adiabatic connection integrand, with $\Psi_\lambda[\rho]$ being the wave function that minimizes $\hat{T} + \lambda \hat{V}_{ee}$ while yielding the density ρ, and $U[\rho]$ being the Hartree energy. Most hybrid functionals then employ a simple ansatz for the density-fixed linear adiabatic connection integrand, for example,[73,74]

$$W_\lambda[\rho] = W^{\mathrm{DFA}}_\lambda[\rho] + \left(E_x - E^{\mathrm{DFA}}_x\right)(1-\lambda)^{n-1}, \tag{3}$$

where DFA denotes a density functional approximation (i.e., a semilocal functional), E_x denotes the Hartree-Fock exchange functional, and n is a parameter. Substituting Eq. (3) into Eq. (2) yields the usual linear mixing between the exact exchange and the density functional approximation with $a = 1/n$. However, Eq. (3) is a quite arbitrary expression for W_λ. It only satisfies the constraint that $W_0 = E_x$ but for $\lambda \neq 0$, it incorporates no exact information and it is not even recovering the correct weak-interaction limit behavior. Thus, most of the accuracy of hybrids relies on the empiricism included into the parameter n and the DFA. This seems to work well for main-group molecular systems but not for other systems such as metal clusters considered here.

A possible non-empirical route that allows us to overcome the limitations of a fixed mixing parameter is the original idea of Seidl and co-workers[75–77] to build a model for the adiabatic-connection integrand of Eq. (2) by interpolating between the known weak- and strong-coupling limits,[78,79]

$$W_{\lambda\to 0}[\rho] = W_0[\rho] + \lambda W'_0[\rho] + \cdots, \tag{4}$$

$$W_{\lambda\to\infty}[\rho] = W_\infty[\rho] + \frac{W'_\infty[\rho]}{\sqrt{\lambda}} + \cdots, \tag{5}$$

where

$$W_0[\rho] = E_x[\rho], \tag{6}$$

$$W'_0[\rho] = 2E^{\mathrm{GL2}}_c[\rho], \tag{7}$$

with E^{GL2}_c being the second-order Görling-Levy (GL) correlation energy,[78] whereas $W_\infty[\rho]$ is the indirect part of the minimum expectation value of the electron-electron repulsion in a given density,[80,81] and $W'_\infty[\rho]$ is the potential energy of coupled zero-point oscillations.[79,80] The idea is that by using a function of λ able to link the result from perturbation theory with the $\lambda \to \infty$ expansion of $W_\lambda[\rho]$, an approximate resummation of the perturbative series is obtained.[76]

The exact $W_\infty[\rho]$ and $W'_\infty[\rho]$ are highly nonlocal density functionals[79,81] that were approximated in the original work of Seidl and co-workers[76,77] by the semilocal point-charge-plus-continuum (PC) model (see the Appendix). As a result, a series of XC functionals can be derived depending on the chosen interpolating function and on whether the $\lambda \to \infty$ expansion includes or not the order $1/\sqrt{\lambda}$: Interaction Strength Interpolation (ISI)[75–77,82] and Revised ISI (revISI)[79] also include $W'_\infty[\rho]$, while Seidl-Perdew-Levy (SPL)[83] and Liu-Burke (LB)[84] only include $W_\infty[\rho]$. They are briefly described in the Appendix. These functionals, which are all based on an adiabatic connection integrand interpolation (ACII), will be generally referred to as ACII functionals. They are non-empirical in the sense that they are approximate perturbation-theory resummations, include full exact exchange, and describe correctly correlation in the weak-interaction limit. Therefore, they are well-suited to try to overcome the limitations of semilocal and hybrid DFT approaches. Their most severe problem could be the lack of size consistency for species made of different atoms, an error that is absent in the case of homogeneous clusters. Moreover, the size consistency issue is actually quite subtle[85,86] and can be corrected in many cases.

The ACII functionals have been rarely tested on systems of interest for practical applications, with the exception of a recent assessment of the ISI functional for main-group chemistry.[82] This investigation has revealed interesting features of this functional and suggested possibilities for future applications.

In this paper, we move away from main group chemistry to assess different ACII functionals for the description of the electronic properties of noble metal clusters, made up of gold and silver. As we have mentioned above, these are very important systems for materials science and chemical applications but their proper computational description is still a challenge. Thus, the testing of high-level DFT methods for this class of systems has a great practical interest. Moreover, the application of non-empirical XC functionals, constructed on a well-defined theoretical framework, to the challenging problem of the simulation of electronic properties of noble metal clusters can help us to highlight new properties and limitations of such approaches. In fact, the next step forward could be to model the adiabatic connection integrand locally[87–89] by interpolating between the exact exchange energy density and the $\lambda \to \infty$ one, for which exact results[90] and approximations compatible with the exact exchange energy density have been recently designed.[91–93] In order to be compatible with the exact exchange energy density, these approximations are non-local and thus more expensive than the semilocal PC functionals (which suffer from the usual gauge problem that arises when we want to combine semilocal functionals with the exact exchange energy density and thus cannot be used in this framework). It has been found that the local interpolations are in general more accurate than their global counterpart.[89] Thus, the study carried out here provides also a very useful first idea of what could be achieved with these higher-level approaches.

II. COMPUTATIONAL DETAILS

In this work, we have tested four ACII XC functionals, which are based on an interpolation of the density-fixed linear adiabatic connection integrand, namely, ISI,[75–77,82]

revISI,[79] SPL,[83] and LB[84] (see the Appendix for details). Additionally, for comparison, we have included results from the Perdew-Burke-Ernzerhof (PBE)[94] and the PBE0[73,95] functionals, which are among the most used semilocal and hybrid functionals, respectively, as well as from the B2PLYP double hybrid functional,[96] which also includes a fraction of second-order Møller-Plesset correlation energy (MP2). We have also considered a comparison with the second-, third-, and fourth-order Møller-Plesset perturbation theory (MP2, MP3, MP4)[56] results. This is because, as explained, the ACII functionals can be seen as an approximate resummation of perturbation theory so that it is interesting to compare them with the first few lower orders. The reference results used in the assessment are specified below for each test set considered:

- **Small gold clusters.** This set consists of the Au_2, Au_2^-, Au_3, Au_3^+, Au_3^-, and Au_4 clusters. For all these systems, we have calculated the atomization energies; for the anions as well as for Au_3 we have computed the ionization potential (IP) energies. The geometries of all clusters have been taken from Ref. 33; they are shown in Fig. 1. Reference energies have been calculated at the coupled cluster singles doubles and perturbative triples [CCSD(T)] level of theory.[97–100]
- **Small silver clusters.** This set includes Ag_2, Ag_2^+, Ag_2^-, Ag_3, Ag_3^+, Ag_3^-, and Ag_4. As for the small gold clusters case, we have computed the atomization energies of all the silver clusters and the IP of the anions as well as of Ag_3. The geometries of all systems have been taken from Ref. 38; they are shown in Fig. 1. Reference values for the energies have been obtained from CCSD(T)[97–100] calculations.
- **Binary gold-silver clusters.** This set considers the AuAg, $AuAg^-$, Au_2Ag, Au_2Ag^-, $AuAg_2$, and $AuAg_2^-$ clusters. Atomization energies have been calculated for all system, while IPs have been computed for the anions. Note that for the anions, we considered as atomization energy the average with respect to the two possible dissociation channels, that is, $AuAg^- \rightarrow Au + Ag^-$ and $AuAg^- \rightarrow Au^- + Ag$; $Au_2Ag^- \rightarrow Au_2 + Ag^-$ and $Au_2Ag^- \rightarrow Au_2^- + Ag$; $AuAg_2^- \rightarrow Au + Ag_2^-$ and $AuAg_2^- \rightarrow Au^- + Ag_2$. The geometries of the binary clusters have been obtained considering the structures reported in Ref. 101 (see Fig. 1) and optimizing them at the revTPSS/def2-QZVP level of theory.[102,103] For these systems, in fact no high-level or experimental geometries are available, except for AuAg. The bond length of the latter (2.496 Å)[104] has been found to be well reproduced by revTPSS/def2-QZVP calculations (2.500 Å). This approach has then been applied to optimize all the binary clusters. Reference energies have been calculated at the CCSD(T) level of theory.[97–100]
- **Gold 2D-3D crossover.** This set includes the Au_{11}^-, Au_{12}^-, and Au_{13}^- clusters that are involved in the two- to three-dimensional crossover of gold clusters. The geometries of all systems have been taken from Ref. 50 and are shown in Fig. 2.
- **Silver 2D-3D crossover.** This set consists of the Ag_5^+, Ag_6^+, and Ag_7^+ clusters, which are relevant to study the two- to three-dimensional crossover of silver clusters. Geometries have been obtained optimizing at the revTPSS/def2-QZVP level of theory,[102,103] the lowest lying structures reported in Ref. 38. The structures are reported in Fig. 2.

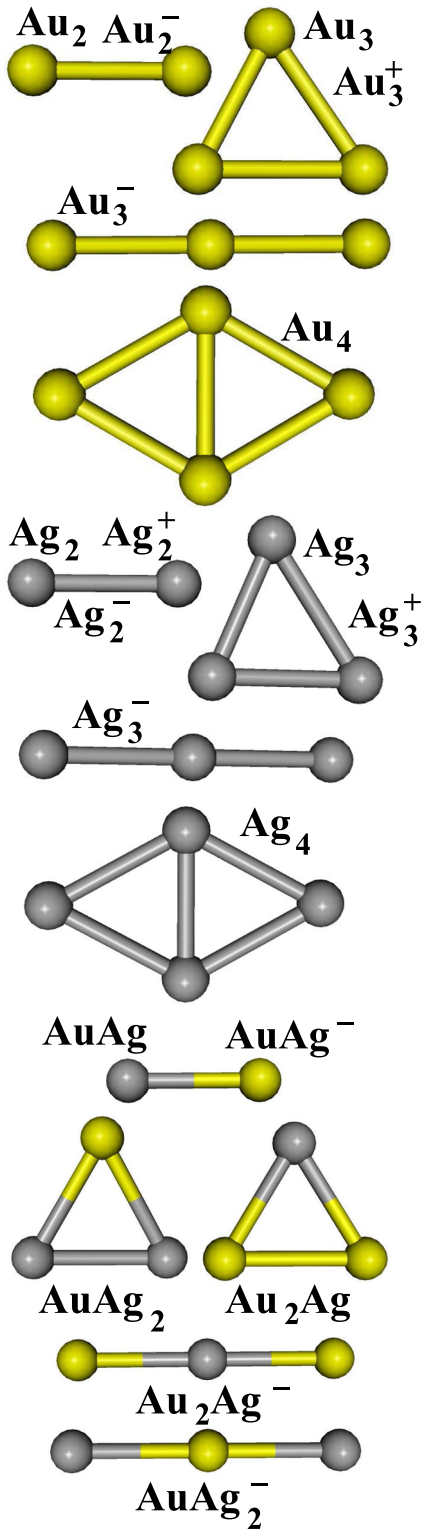

FIG. 1. Structures of the small gold, silver, and binary gold-silver clusters.

Because accurate experimental data are not available for all the systems, our assessment of the performances of the ACII functionals on small clusters is carried out w.r.t. CCSD(T)

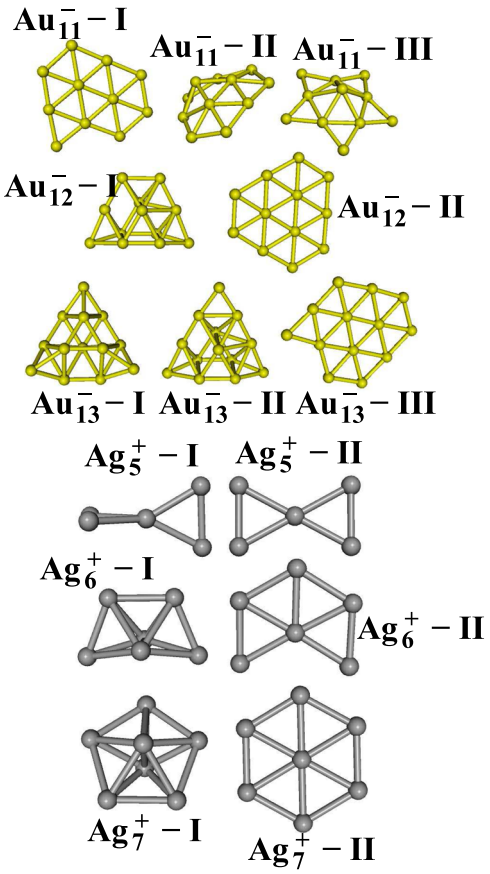

FIG. 2. Structures of the gold and silver clusters considered for the 2D-3D dimensional crossover problem.

values. This allows a more direct and sensible comparison of the results, whereas the comparison with experimental data would require the consideration of further effects such as thermal/vibronic ones as well as spin-orbit coupling.[33,50] Of course, CCSD(T) results cannot generally be considered "exact" for metal clusters. Nevertheless, for very small clusters, as those considered in our study, CCSD(T) is usually considered a reliable reference.[32,33,38,67,69,105–110] Indeed, in all our CCSD(T) calculations, the value of the D_1 diagnostic,[111,112] designed to measure the multi-reference character of the CCSD ground state, was always smaller than 0.1. Similarly, the percentage variation of the total interaction energy due to the inclusion of perturbative triples (%TAE),[113] which is an indicator for both multi-reference and truncation error limitations, was always lower than or equal to 10%. Both values are therefore within the values considered acceptable for CCSD(T) ($D_1 \approx 0.15$ and %TAE ≈ 10).[113] Finally, for the energy differences considered in this paper, we could estimate the employed basis set (aug-cc-pwCVQZ-PP, see below) to be converged below 0.05 eV. Thus, we can expect no significant problem in evaluating interaction energies with our CCSD(T) protocol.

Actually, an accurate comparison with available experimental data from the literature shows that, for atoms (regarding ionization energies)[114,115] and neutral dimers and trimers (regarding both ionization and atomization energies),[116–118] our CCSD(T) results are within 0.04 eV from the experimental ones; for the charged dimers and trimers (regarding both ionization and atomization energies), our CCSD(T) results are within 0.2 eV from experimental data.[115,119,120] Thus, the agreement is very good for neutral clusters/atoms and reasonable for charged species. We note that this larger discrepancy may be partly ascribable to a diminished accuracy of the CCSD(T) calculation *per se* in these cases, but it may also be possibly due to the rather large error bars associated with the measures on the experimental side and on the increased importance of correcting terms on the computational side. This shows, in conclusion, that no significant truncation and/or basis set errors are present and our reference CCSD(T) data are sufficiently converged for the purpose of this study.

Concerning the 2D-3D crossover of both gold and silver clusters, no exact experimental energies are available for a quantitative comparison. Moreover, for these systems, we could not afford accurate CCSD(T) calculations (whose accuracy, for such relatively large clusters, would also be uncertain). Therefore, for these cases, we do not provide reference values and we consider only a qualitative analysis. Nevertheless, in order to provide some quantitative indication of the performance of the functionals, we report for the 2D-3D crossover the results of meta-GGA DFT calculations performed with the balanced localization (BLOC) functional.[121–123] Recent studies have indeed shown that this is a quite accurate approach for this problem.[121] We remark anyway that these results cannot be considered accurate benchmarks but should be rather used as a comparison with a reasonably accurate computational approach.

All the required calculations have been performed with the TURBOMOLE program package,[124,125] employing, unless otherwise stated, the aug-cc-pwCVQZ-PP basis set[126] and a Stuttgart-Koeln MCDHF 60-electron effective core potential.[127] The calculations concerning the ISI, revISI, SPL, and LB functionals have been performed in a post-self-consistent-field (post-SCF) fashion, using Hartree-Fock orbitals. This computational scheme is discussed in details in Ref. 82. In particular, our choice is motivated by the empirical observation that the ISI functional yields much better results when used as a correlation correction for the HF energy. The PBE and PBE0 calculations have been performed using a full SCF procedure; B2PLYP calculations have been carried out as described in Ref. 96, considering a SCF treatment of the exchange and semilocal correlation part and adding the second-order MP2 correlation fraction as a post-SCF correction.

III. RESULTS

In this section, we analyze the performance of the ACII XC functionals for the description of the electronic properties of gold, silver, and mixed Au/Ag clusters. The results are compared to those obtained from other approaches, such as semilocal and hybrid DFT as well as wave-function perturbation theory.

A. Total energies

To start our investigation, we consider, in Table I, the errors on total energies computed with different methods

TABLE I. Errors on total energies (eV/atom) of small gold, silver, and binary clusters. For each set of clusters, the mean absolute error (MAE) is reported. In the bottom part of the table, we report also the statistics for the overall set [mean error (ME), MAE, and standard deviation].

	PBE	PBE0	B2PLYP	ISI	revISI	SPL	LB	MP2	MP3	MP4
Au	−4.93	−3.75	−1.73	2.84	2.93	2.65	1.97	−0.33	0.98	−0.27
Au+	−4.58	−3.73	−1.64	2.63	2.70	2.50	1.89	−0.10	0.68	−0.15
Au−	−4.94	−3.47	−1.65	3.26	3.38	3.02	2.25	−0.35	1.44	−0.41
Au2	−4.96	−3.66	−1.69	2.89	2.99	2.67	1.94	−0.53	1.22	−0.43
Au2−	−4.97	−3.58	−1.66	3.06	3.17	2.83	2.08	−0.46	1.40	−0.44
Au3	−4.97	−3.65	−1.67	2.89	3.00	2.67	1.94	−0.54	1.29	−0.48
Au3+	−4.90	−3.68	−1.66	2.80	2.90	2.59	1.88	−0.50	1.15	−0.43
Au3−	−4.94	−3.54	−1.66	2.98	3.10	2.73	1.96	−0.65	1.40	−0.55
Au4	−4.96	−3.62	−1.67	2.86	2.97	2.63	1.87	−0.66	1.33	−0.54
ME	−4.91	−3.63	−1.67	2.91	3.01	2.70	1.97	−0.46	1.21	−0.41
MAE	4.91	3.63	1.67	2.91	3.01	2.70	1.97	0.46	1.21	0.41
Ag	−0.89	−0.36	0.21	3.24	3.39	2.91	2.18	−0.26	1.04	−0.27
Ag+	−0.44	−0.25	0.38	2.99	3.13	2.71	2.04	−0.19	0.76	−0.20
Ag−	−0.99	−0.21	0.24	3.68	3.85	3.31	2.53	−0.08	1.39	−0.32
Ag2	−0.96	−0.30	0.22	3.32	3.49	2.97	2.19	−0.37	1.18	−0.38
Ag2+	−0.79	−0.34	0.28	3.14	3.28	2.82	2.11	−0.26	0.95	−0.27
Ag2−	−1.00	−0.27	0.24	3.50	3.67	3.14	2.37	−0.22	1.34	−0.33
Ag3	−0.95	−0.30	0.25	3.32	3.49	2.96	2.19	−0.39	1.23	−0.40
Ag3+	−0.85	−0.30	0.27	3.21	3.37	2.86	2.11	−0.41	1.10	−0.38
Ag3−	−0.97	−0.23	0.25	3.45	3.63	3.07	2.27	−0.38	1.32	−0.43
Ag4	−0.95	−0.27	0.24	3.29	3.47	2.91	2.12	−0.51	1.24	−0.45
ME	−0.88	−0.28	0.26	3.31	3.48	2.97	2.21	−0.31	1.15	−0.34
MAE	0.88	0.28	0.26	3.31	3.48	2.97	2.21	0.31	1.15	0.34
AuAg	−2.93	−1.95	−0.72	3.10	3.24	2.81	2.06	−0.47	1.20	−0.41
AuAg−	−2.97	−1.91	−0.70	3.27	3.41	2.97	2.20	−0.37	1.36	−0.39
Au_2Ag	−3.58	−2.49	−1.00	3.03	3.16	2.76	2.01	−0.51	1.28	−0.46
Au_2Ag^-	−3.57	−2.40	−1.00	3.14	3.28	2.84	2.06	−0.57	1.36	−0.50
$AuAg_2$	−2.26	−1.38	−0.37	3.18	3.33	2.86	2.10	−0.46	1.26	−0.43
$AuAg_2^-$	−2.32	−1.34	−0.40	3.30	3.46	2.96	2.18	−0.46	1.36	−0.47
ME	−2.94	−1.91	−0.70	3.17	3.31	2.87	2.10	−0.47	1.30	−0.44
MAE	2.94	1.91	0.70	3.17	3.31	2.87	2.10	0.47	1.30	0.44
					Overall statistics					
ME	−2.82	−1.88	−0.66	3.13	3.27	2.85	2.10	−0.40	1.21	−0.39
MAE	2.82	1.88	0.87	3.13	3.27	2.85	2.10	0.40	1.21	0.39
Std. dev.	1.81	1.51	0.87	0.24	0.27	0.18	0.16	0.15	0.20	0.10

with respect to the CCSD(T) reference values. Although this quantity is usually not of much interest in practical applications (where energy differences are usually considered), the analysis of the errors on total energies will be useful to understand the performances of the different functionals for more practical properties such as atomization or ionization energies.

Inspection of the data shows that the ACII functionals do not perform very well for the total energy. In fact, they yield the highest mean absolute errors (MAEs), being even slightly worse than the semilocal PBE approach and giving definitely larger errors with respect to perturbation theory (MP2, MP3, and MP4) and to the double hybrid B2PLYP functional. Among the ACII functionals, the SPL and especially the LB approach perform systematically better than ISI and revISI. Thus LB yields errors that are often 30% smaller than ISI, even though they are still usually larger than those of the other non-ACII methods. On the other hand, considering the standard deviation of the errors (last line of Table I), we note that the ACII results display a quite small dispersion around the average (with LB and SPL again slightly better than ISI and revISI). This is related to the fact that the ACII functionals all give a quite systematic underestimation (in magnitude) of the energy of all systems. By contrast, PBE, PBE0, and partly B2PLYP give larger values of the standard deviation. This depends on the fact that these methods describe quite accurately some systems (e.g., Ag clusters), which are the ones that effectively contribute to produce a quite low MAE, but they give significantly larger errors for other systems. This behavior is a signature of the too simplistic nature of these functionals, which cannot capture equally well the physics of all systems.

The observed standard deviations suggest that when energy differences are considered, the ACII functionals can

benefit from a cancellation of the systematic error such that rather accurate energy differences can be obtained. We must remark also that the standard deviation values reported in Table I allow only a partial understanding of the problem because they are obtained from all the data but, depending on the property of interest, some energy differences may be more relevant than others, e.g., for atomization energies, the difference between a cluster energy and the energy of the composing atoms is the most relevant. Thus, for example, MP methods all yield quite low standard deviations, but a closer look at the results shows that the errors for atoms are quite different than those for the clusters (much more different than for ACII methods); hence, we can expect that despite a quite good MAE and a small standard deviation, MP2, MP3, and MP4 atomization energies can display a limited accuracy. A more detailed analysis of the relationship between the data reported in Table I and some relevant energy difference properties will be given in Sec. IV.

B. Atomization and ionization energies

A first example of an important energy difference is the atomization energy. The atomization energy values calculated for the sets of gold, silver, and binary clusters with all the methods are reported in Table II. Observing the data, it appears that as anticipated, for atomization energies, the ACII functionals work fairly well. In particular, SPL and LB yield mean absolute relative errors (MAREs) of about 2%–3% for all kinds

TABLE II. Atomization energies (eV) of small gold, silver, and binary clusters. Note that for anionic binary clusters, the average between the two possible dissociation paths has been considered (see Sec. II). For each set of clusters, the mean error (ME), the mean absolute error (MAE), the mean absolute relative error (MARE), and the standard deviation are reported. In the bottom part of the table, we report also the statistics for the overall set.

	PBE	PBE0	B2PLYP	ISI	revISI	SPL	LB	MP2	MP3	MP4	CCSD(T)
Au_2	2.33	2.08	2.20	2.17	2.14	2.24	2.33	2.67	1.79	2.60	2.27
Au_2^-	1.97	1.83	1.83	1.86	1.84	1.90	1.95	2.14	1.51	2.09	1.89
Au_3	3.57	3.14	3.26	3.28	3.23	3.39	3.54	4.08	2.51	4.07	3.45
Au_3^+	6.06	5.60	5.67	5.71	5.66	5.82	5.97	6.54	4.98	6.38	5.79
Au_3^-	4.90	4.52	4.73	4.87	4.81	5.00	5.17	5.80	4.05	5.57	4.87
Au_4	6.18	5.51	5.81	5.95	5.85	6.14	6.40	7.37	4.60	7.10	6.03
ME	0.12	–0.27	–0.14	–0.08	–0.13	0.03	0.18	0.71	–0.81	0.58	
MAE	0.12	0.27	0.14	0.08	0.13	0.06	0.18	0.71	0.81	0.58	
MARE (%)	3	7	3	2	4	1	4	17	21	14	
Std. dev.	0.08	0.16	0.06	0.06	0.07	0.08	0.13	0.39	0.37	0.30	
Ag_2	1.82	1.59	1.69	1.53	1.50	1.59	1.66	1.93	1.41	1.91	1.70
Ag_2^+	1.85	1.69	1.64	1.58	1.57	1.59	1.61	1.70	1.51	1.67	1.62
Ag_2^-	1.53	1.39	1.37	1.32	1.31	1.35	1.38	1.51	1.15	1.48	1.41
Ag_3	2.73	2.37	2.45	2.31	2.27	2.41	2.52	2.94	2.00	2.94	2.56
Ag_3^+	4.84	4.45	4.50	4.36	4.32	4.47	4.59	5.03	4.05	4.90	4.52
Ag_3^-	3.70	3.32	3.49	3.38	3.32	3.50	3.63	4.12	3.06	4.01	3.57
Ag_4	4.80	4.24	4.47	4.39	4.30	4.58	4.80	5.59	3.78	5.28	4.59
ME	0.19	–0.13	–0.05	–0.16	–0.20	–0.07	0.03	0.41	–0.43	0.32	
MAE	0.19	0.15	0.06	0.16	0.20	0.07	0.06	0.41	0.43	0.32	
MARE (%)	7	5	2	6	7	3	2	13	15	10	
Std. dev.	0.07	0.14	0.06	0.07	0.09	0.05	0.09	0.32	0.23	0.22	
AuAg	2.22	1.97	2.11	2.05	2.02	2.13	2.21	2.53	1.80	2.46	2.18
$AuAg^-$	1.83	1.69	1.71	1.74	1.72	1.78	1.83	2.00	1.47	1.92	1.77
Au_2Ag	3.65	3.26	3.42	3.47	3.41	3.59	3.73	4.28	2.80	4.22	3.65
Au_2Ag^-	4.96	4.58	4.84	4.97	4.91	5.12	5.28	5.90	4.36	5.63	5.04
$AuAg_2$	3.33	2.94	3.08	3.06	3.00	3.17	3.30	3.80	2.56	3.75	3.28
$AuAg_2^-$	3.83	3.40	3.58	3.48	3.42	3.60	3.74	4.25	3.00	4.14	3.63
ME	0.04	–0.29	–0.14	–0.13	–0.18	–0.03	0.09	0.53	–0.60	0.43	
MAE	0.07	0.29	0.14	0.13	0.18	0.06	0.09	0.53	0.60	0.43	
MARE (%)	2	9	4	4	6	2	3	16	19	13	
Std. dev.	0.09	0.14	0.08	0.07	0.08	0.06	0.08	0.23	0.21	0.18	
Overall statistics											
ME	0.12	–0.22	–0.11	–0.12	–0.17	–0.02	0.10	0.54	–0.60	0.44	
MAE	0.13	0.23	0.11	0.12	0.17	0.06	0.11	0.54	0.60	0.44	
MARE (%)	4	7	3	4	6	2	3	15	18	12	
Std. dev.	0.10	0.16	0.08	0.07	0.08	0.07	0.11	0.33	0.31	0.25	

of clusters, being competitive with the B2PLYP functional. The ISI and revISI functionals perform slightly worse, displaying a systematic underbinding and giving overall MAREs of 4% and 6%, respectively. Moreover, unlike for SPL and LB, non-negligible differences exist in the description of the different materials with gold clusters described better than silver ones. Overall the ISI and revISI functionals show a comparable performance as PBE and better than PBE0. Finally, the MP results show a quite poor performance, exhibiting MAREs ranging form 10% to 20%. In addition, we can note that MP2 results are closer to MP4 results than MP3 ones not only from a quantitative point of view but also qualitatively (MP2 and MP4 always overbind, while MP3 always consistently underbinds). This is a clear indication of the difficult convergence of the perturbative series for the metal clusters electronic properties.

In Table III, we report the computed ionization potential energies, which are other important energy differences to consider for metal clusters. In this case, the ACII functionals perform rather poorly, being the worst methods, if we exclude MP3. As in the case of atomization energies, SPL and LB (especially the latter) show a slightly better performance than ISI and revISI. Nevertheless, the results are definitely worse than for B2PLYP, PBE, and even PBE0. A rationalization of this failure will be given is Sec. IV.

C. 2D-3D crossover

To conclude this section, we consider the problem of the two- to three-dimensional (2D-3D) crossover of anionic gold clusters and cationic silver clusters. Different studies have indicated that for anionic gold clusters, the dimensional crossover occurs between Au_{11}^- (2D) and Au_{13}^- (3D), with the 2D and 3D Au_{12}^- structures being almost isoenergetic.[49,50] On the other hand, for cationic silver clusters, it has been suggested that the dimensional transition occurs already for Ag_5^+, which has a 2D structure with a slightly lower energy than the 3D one, while Ag_6^+ and Ag_7^+ display lowest energy 3D structures.[39,128] Anyway, this is a quite difficult problem because experimentally it is not trivial to distinguish clusters

TABLE III. Ionization potentials (eV) of small gold, silver, and binary clusters. For each set of clusters, the mean error (ME), the mean absolute error (MAE), the mean absolute relative error (MARE), and the standard deviation are reported. In the bottom part of the table, we report also the statistics for the overall set.

	PBE	PBE0	B2PLYP	ISI	revISI	SPL	LB	MP2	MP3	MP4	CCSD(T)
Au	9.54	9.22	9.29	9.00	8.97	9.05	9.13	9.42	8.91	9.32	9.20
Au^-	2.30	2.00	2.21	1.86	1.84	1.92	2.01	2.31	1.82	2.42	2.29
Au_2^-	1.94	1.75	1.84	1.56	1.55	1.58	1.62	1.78	1.53	1.91	1.91
Au_3	7.05	6.76	6.89	6.57	6.55	6.62	6.69	6.97	6.44	7.01	6.86
Au_3^-	3.63	3.38	3.67	3.45	3.41	3.53	3.63	4.03	3.36	3.92	3.70
ME	0.10	–0.17	–0.01	–0.30	–0.33	–0.25	–0.17	0.11	–0.38	0.12	
MAE	0.13	0.18	0.06	0.30	0.33	0.25	0.17	0.16	0.38	0.12	
MARE (%)	2	6	2	10	11	9	6	4	12	3	
Std. dev.	0.17	0.14	0.07	0.08	0.08	0.09	0.11	0.18	0.07	0.08	
Ag	8.04	7.70	7.76	7.35	7.33	7.40	7.45	7.67	7.31	7.66	7.59
Ag^-	1.40	1.15	1.28	0.86	0.85	0.90	0.95	1.13	0.95	1.35	1.31
Ag_2	8.02	7.60	7.80	7.30	7.26	7.40	7.50	7.90	7.21	7.90	7.68
Ag_2^-	1.11	0.96	0.97	0.66	0.65	0.66	0.67	0.72	0.69	0.92	1.01
Ag_3	5.93	5.63	5.71	5.30	5.28	5.34	5.39	5.58	5.26	5.70	5.64
Ag_3^-	2.38	2.10	2.32	1.93	1.90	1.99	2.06	2.31	2.02	2.42	2.31
ME	0.22	–0.06	0.05	–0.36	–0.38	–0.31	–0.25	–0.04	–0.35	0.07	
MAE	0.22	0.10	0.07	0.36	0.38	0.31	0.25	0.14	0.35	0.10	
MARE (%)	6	5	2	17	17	15	13	8	15	4	
Std. dev.	0.16	0.11	0.08	0.07	0.07	0.07	0.09	0.18	0.07	0.10	
$AuAg^-$	1.46	1.30	1.35	1.05	1.04	1.07	1.09	1.19	1.07	1.34	1.39
Au_2Ag^-	3.16	2.90	3.17	2.87	2.84	2.94	3.03	3.34	2.95	3.30	3.18
$AuAg_2^-$	2.35	2.04	2.24	1.79	1.76	1.84	1.91	2.17	1.83	2.28	2.15
ME	0.09	–0.16	0.01	–0.34	–0.36	–0.29	–0.23	–0.01	–0.29	0.07	
MAE	0.10	0.16	0.05	0.34	0.36	0.29	0.23	0.13	0.29	0.10	
MARE (%)	5	7	3	17	18	15	12	7	15	4	
Std. dev.	0.11	0.11	0.07	0.03	0.03	0.04	0.07	0.18	0.05	0.10	
Overall statistics											
ME	0.15	–0.12	0.02	–0.33	–0.36	–0.28	–0.22	0.02	–0.35	0.09	
MAE	0.16	0.14	0.06	0.33	0.36	0.28	0.22	0.15	0.35	0.11	
MARE (%)	4	6	2	14	15	13	11	6	14	4	
Std. dev.	0.16	0.12	0.08	0.07	0.07	0.07	0.09	0.18	0.07	0.09	

TABLE IV. Relative energies (eV) with respect to conformer I (see Sec. II) of 2D and 3D anionic gold clusters and cationic silver clusters. For the gold clusters, the data include the correction terms reported in Table IV of Ref. 50.

		PBE	PBE0	BLOC	B2PLYP	ISI	revISI	SPL	LB	MP2
Au_{11}^--I	2D	...	...	...	...	...	...	...	...	...
Au_{11}^--II	3D	0.217	0.224	0.206	0.147	0.083	0.090	0.070	0.054	−0.006
Au_{11}^--III	3D	0.270	0.179	0.354	0.254	0.265	0.251	0.302	0.344	0.499
Au_{12}^--I	3D	...	...	...	...	...	...	...	...	...
Au_{12}^--II	2D	−0.450	−0.340	0.008	−0.144	0.710	0.669	0.789	0.882	1.228
Au_{13}^--I	3D	...	...	...	...	...	...	...	...	...
Au_{13}^--II	3D	−0.027	−0.032	0.037	−0.024	0.497	0.495	0.499	0.527	0.618
Au_{13}^--III	2D	−0.111	0.056	0.386	0.248	0.802	0.894	0.917	0.824	1.069
Ag_5^+-I	3D	...	...	...	...	...	...	...	...	...
Ag_5^+-II	2D	0.021	0.025	0.024	0.020	0.021	0.020	0.018	0.017	0.013
Ag_6^+-I	3D	...	...	...	...	...	...	...	...	...
Ag_6^+-II	2D	−0.005	0.055	0.280	0.007	0.220	0.211	0.241	0.265	0.348
Ag_7^+-I	3D	...	...	...	...	...	...	...	...	...
Ag_7^+-II	2D	−0.099	...	0.303	−0.059	0.286	0.270	0.318	0.352	0.474

of the same size but different dimensionality. A computational support is thus required.[39,48–50,128,129] However, to describe correctly the energy ordering of several noble metal clusters with very similar energies is a hard task for any computational method.[33,50,121,130] For this reason, this is a very interesting problem from the computational point of view.

In Table IV, we report the energies calculated for the anionic gold clusters and cationic silver clusters relevant for the 2D-3D transition. Because no reliable benchmark values can be obtained for these clusters, the table does not report any reference values. Anyway, to provide some comparison, we have listed the results obtained with the BLOC meta-GGA functional,[121–123] which is expected to be a quite accurate approach for this kind of problems.[121] Observing the data, one can immediately note that the PBE, PBE0, and even B2PLYP methods are not reliable for the dimensional crossover of noble metal clusters. In fact, PBE always favors 2D structures, whereas PBE0 predicts the 2D-3D transition at a too large cluster dimension for gold, Au_{13}^- (although the 3D geometry with lowest energy is not the same as the one we find with BLOC and all ACII functionals), and for silver, the energies of the 2D and 3D clusters differ slightly for both $n = 6$ and $n = 7$, not evidencing a clear transition at the expected cluster size. A similar behavior is found for the B2PLYP functional, which was instead one of the best for the atomization energies and IPs of small clusters. The ACII functionals overall perform all quite similarly, predicting for all clusters the expected ordering and agreeing well with BLOC results for the cationic Ag clusters but tending to favor 3D structures in the anionic Au clusters. We note that this behavior is somehow inherited from the MP2 method, which however performs much worse than any of the ACII functionals considered here.

IV. DISCUSSION AND ANALYSIS OF THE RESULTS

In Sec. III B, we saw that the ACII functionals perform rather well for the calculation of atomization energies of noble metal clusters. As mentioned above, a good rationalization of the observed results can be obtained in terms of the energy errors that the different methods display for the total energies of atoms and of the clusters. These have been reported in Table I.

A. Energy differences

For a better visualization here, we additionally plot, in Fig. 3, the quantity

$$\delta\Delta E = \Delta E(M_n M_m^- M_l^+) - \sum_n \Delta E(M_n) - \sum_m \Delta E(M_n^-) - \sum_l \Delta E(M_n^+), \quad (8)$$

where ΔE are the total energy errors (the ΔE per atom are reported in Table I), M = Au or Ag, and n, m, l are the integers such that $M_n M_m^- M_l^+$ corresponds to a given cluster (e.g., for Au_3^+ we have M = Au, $n = 2$, $m = 0$, and $l = 1$). This quantity provides a measure of how different is the energy error made on a given cluster from that of its constituent atoms. Inspection of

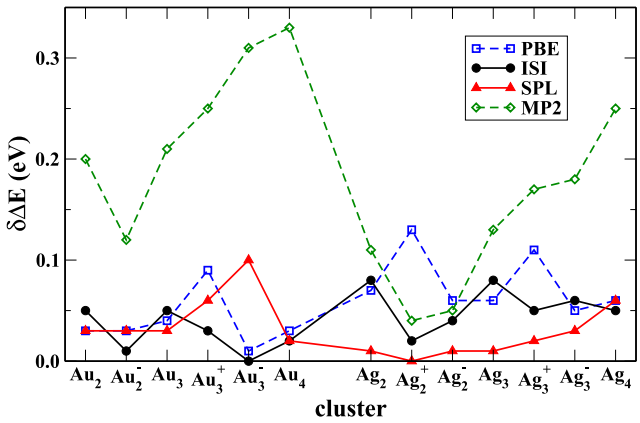

FIG. 3. Difference in the total energy error between a cluster and its constituent atoms [see Eq. (8)].

the plots shows that the smaller $\delta\Delta E$ values are yielded by the ISI and SPL (revISI and LB, not reported, give similar results). These functionals are also among the best performers for the atomization energies. On the other hand, for PBE we observe that the $\delta\Delta E$ is small for gold clusters, with the exception of Au_3^+, while for silver clusters it is larger. Indeed, looking to Table II we can find that PBE performs well for gold clusters, with the exception of Au_3^+ that yields an error of 0.27 eV (more than twice larger than the MAE), while it performs less well for silver clusters. Finally, for MP2 the values of $\delta\Delta E$ are generally very large. Thus, despite MP2 is on average quite accurate in the description of the total energies (see Table I), it fails to produce accurate atomization energies because of accumulation of the errors.

A similar analysis can be made to comment the results of the ionization potential calculations (reported in Table III). However, in this case, the difference to consider is between the neutral and the charged species. Then, a different behavior is observed. In fact, while for most of the considered methods, the total energy error is not much different between a neutral and a charged species of the same cluster, for the ACII functionals we always observe an increase of the error with the charge. This situation is schematized in Fig. 4, where we plot, for several examples, the quantity

$$\Delta(q) = \Delta E(A^q) - \Delta E(A^0)\,, \tag{9}$$

with A being any of the systems under investigation and $q = -1, 0, 1$. The observed trend may trace back to a different ability of ACII functionals to describe the high- and low-density regimes. As a consequence, the ACII functionals are generally the worst performers for the calculation of ionization potentials, while PBE and especially B2PLYP perform well thanks to the more homogenous description of the differently charged species.

This analysis shows that although the quality of the total energies produced by a functional is a key element to understand the performance of the functional, the basic property to observe is not the quality of the absolute energies, but rather the variance of the errors. Furthermore, the contrasting behaviors we have observed for the description of the atomization energies and of the ionization potentials highlight the subtleties inherent to such calculations. In particular, the accuracy of the ACII functionals has been shown to be not much dependent on the investigated material (Au or Ag) nor on the system's size but to be quite sensitive to the charge state of the computed system. The first feature is a positive one. This is related, as we saw, to the computation of atomization energies, but even more importantly it indicates that the idea beyond the construction of the ACII functionals is in general quite robust such that the functionals although not very accurate in absolute terms (see Table I) are well transferable to systems of different size and composition. This is not a trivial results since, as we documented, other methods (e.g., PBE and PBE0, but even MP4) do not share this property. On the contrary, the dependence of the ACII functionals on the charge state of the system indicates a clear limitation of such approaches. They are in fact unable to describe with similar accuracy systems with qualitatively different charge distributions. As a consequence, the ionization potential calculations are problematic for ACII functionals.

B. AC curves: Gold dimer showcase

To rationalize the origin of the limitations of the ACII functionals as well as to understand in depth the differences and the similarities between the different interpolation formulas, it would be necessary to inspect in some detail the shape of the density-fixed linear adiabatic connection integrand defining ISI, revISI, SPL, and LB. However, contrary to small atoms and molecules (see, e.g., Refs. 131–133), for noble metal clusters, there exists no reference adiabatic connection integrands to compare to. Thus, such a detailed analysis is not really possible. Nevertheless, some useful hints can be obtained by a semi-qualitative comparison of the various adiabatic connection curves. As an example, in Fig. 5 we report, for the Au_2 case (the other systems studied here have very similar features), the atomization adiabatic connection integrand, defined as

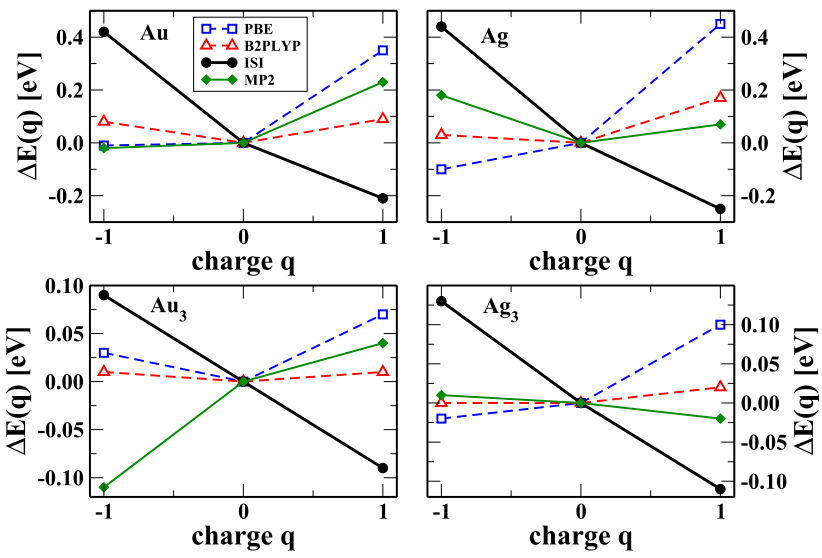

FIG. 4. Variation of the energy error with the total charge of the system (Au top left, Au_3 bottom left, Ag top right, Ag_3 bottom right). The values are scaled to the neutral system value [see Eq. (9)]. Note that only the values $q = -1, 0, +1$ have been computed; these are denoted by the symbols in the plot. The straight lines connecting the symbols have only a graphical purpose, to highlight the trend. They do not represent the behavior for fractional charges.

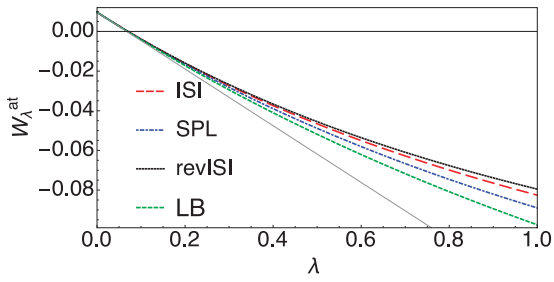

FIG. 5. Atomization adiabatic connection integrands [see Eq. (10)] corresponding to ISI, revISI, SPL, and LB for the Au_2 case; the thick curve in gray corresponds to the linear expansion for the atomization adiabatic connection integrand [Eq. (11)].

$$W_\lambda^{at}(\mathrm{Au_2}) = W_\lambda(\mathrm{Au_2}) - 2W_\lambda(\mathrm{Au})\,, \tag{10}$$

for ISI, revISI, SPL, and LB. The integrated value (between 0 and 1) of this quantity corresponds to the XC atomization energy calculated with a given ACII functional. Note that because the ACII functionals are not size-consistent,[82] slightly different definitions of Eq. (10) could be given. Nevertheless, using the procedure of Refs. 82 and 134, the size-inconsistency error on atomization energies can be estimated to be less than 0.05 eV for all the cases considered in this work. Thus, we expect no observable difference between different definitions of W_λ^{at}. For discussion, we have plotted also the weak interacting limit expansion truncated at linear order in λ for the atomization adiabatic connection integrand, which is defined as

$$W_{\lambda,LE}^{at}(\mathrm{Au_2}) = W_{\lambda,LE}(\mathrm{Au_2}) - 2W_{\lambda,LE}(\mathrm{Au}), \tag{11}$$

where the linear expansion (LE) of the AC integrand for a species X is $W_{\lambda,LE}(\mathrm{X}) = E_x(\mathrm{X}) + 2\lambda E_c^{\mathrm{GL2}}(\mathrm{X})$ in agreement with Eq. (4) and in the case of HF orbitals $E_c^{\mathrm{GL2}}(\mathrm{X}) = E_c^{\mathrm{MP2}}(\mathrm{X})$. Because of the weak-interacting limit constraint, all the curves plotted in the figure share the same $\lambda = 0$ value, which corresponds to the Hartree-Fock exchange atomization energy, as well as the same slope at this point. The curves remain very similar up to $\lambda \approx 0.2$, which is not strictly dictated by the weak-interacting limit constraint but rather by a possible lack of flexibility in the interpolation formulas. For values of $\lambda \gtrsim 0.2$, the curves associated with the various functionals start to differ, due to the different ways they approach the W_∞ value for $\lambda = \infty$. Note that in this case, ISI and revISI are further constrained to recover the W'_∞ slope, whereas SPL and LB do not have this constraint. The interpolation towards the strong-interaction limit is therefore the main feature differentiating the various ACII functionals, even in the range $0 \le \lambda \le 1$. In general, revISI is the slowest to approach the asymptotic W_∞ value, whereas LB is the fastest. So the former will usually yield the smaller XC energies, whereas the latter will produce the larger XC energies (in magnitude). In fact, turning to the Au_2 example reported in Fig. 5, the inspection of the plot shows that revISI is indeed the slowest to move towards the asymptotic W_∞^{at} value (for $\mathrm{Au_2}\, W_\infty^{at} = -0.239$). Consequently, in Table II it yields the smallest atomization energy (it underestimates the Au_2 atomization energy by 0.13 eV). On the opposite, LB is the fastest to move towards the asymptotic W_∞^{at} value, thus it gives the larger atomization energy (overestimating it by 0.06 eV). In this specific case, the SPL functional, which behaves almost intermediately between revISI and LB, yields a very accurate value of the atomization energy, underestimating it by only 0.03 eV.

Thus, we have seen that there are two main features that can determine the performance of an ACII functional. The first one is surely the behavior towards the strong-coupling limit, which is able to influence the shape of the adiabatic connection integrand curve for $\lambda \gtrapprox 0.2/0.3$. This behavior is indeed modeled differently by the various functionals examined in this work, but it appears that none of them can really capture the correct behavior in the range of interest $0.3 \le \lambda \le 1$. This is possibly due to the fact that information on the $\lambda = \infty$ point is not sufficient to guide correctly the interpolation at the quite small λ values of interest for the calculation of XC energies. A second factor that is relevant for the functionals' performance is the small λ behavior. At very small λ values, this is determined by Eq. (4), but for larger values of the coupling constant (at least for $0.1 \le \lambda \le 0.2$), the shape of the curve should depart from the slope given by E_c^{GL2} in order to correctly describe the higher-order correlation effect. Instead, we have observed that all the ACII functionals provide the same behavior up to $\lambda \approx 0.2$. This indicates that the interpolation formulas have not enough flexibility to differentiate from the asymptotic behavior imposed at $\lambda = 0$.

C. Role of the reference orbitals

The ACII functionals are orbital-dependent nonlinear functionals; thus, they are usually employed to compute the XC energy in a post-SCF fashion (as we did in this work). Then, the results depend on the choice of the orbitals used for the calculation. Recent work[82] has evidenced that ISI results for main-group chemistry are much improved when Hartree-Fock orbitals are used. This has been basically traced back to the characteristics of the Hartree-Fock single-particle energy gap (which determines the magnitude of E_c^{GL2} and thus the weak-interaction behavior of the curves).

For gold and silver clusters, after some test calculations, we found a similar result for all the ACII formulas considered. For this reason, all the results reported in Sec. III are based on Hartree-Fock orbitals. To clarify this aspect, we have reported in Fig. 6 both the bare and the atomization adiabatic connection integrands computed with the SPL formula (similar results are obtained for the other formulas) for Au_2 and Au using either Hartree-Fock and PBE orbitals. It can be seen that the adiabatic connection curve of Au_2, obtained from Hartree-Fock orbitals, is very similar to twice the Au curve. Hence, the atomization adiabatic connection integrand is rather flat, yielding (correctly) a moderate atomization XC energy. This behavior depends partly on the fact that in Hartree-Fock calculations Au_2 has almost twice the exchange energy of Au but, primarily, it traces back to the fact that the Au_2 MP2 correlation energy is almost perfectly two times larger than the Au one (which in turn depends on the fact that the two systems have very close single-particle energy gaps

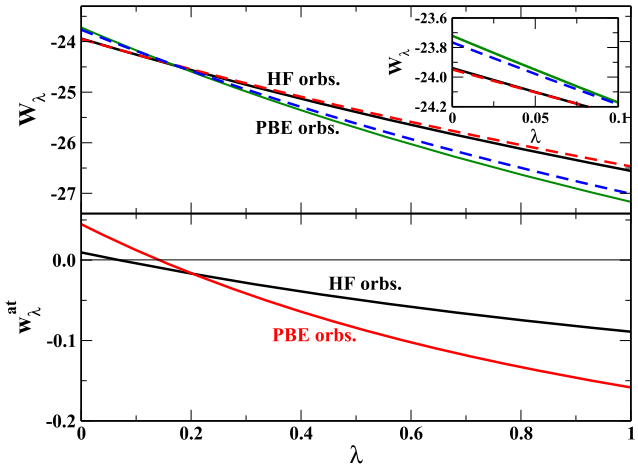

FIG. 6. Top: Adiabatic connection integrands computed with the SPL formula [Eq. (A8)] for Au_2 (solid line) and Au (dashed line) using Hartree-Fock and PBE orbitals; the Au curve is multiplied by a factor of 2; the inset shows the weak-interaction part of the curves. Bottom: Atomization adiabatic connection integrands [see Eq. (10)] computed with the SPL formula for the Au_2 case.

−7.604 eV and 7.707 eV, respectively—and on the size-extensivity of the MP2 method). Thus, the adiabatic connection integrands for Au_2 and twice the Au have almost identical slopes at $\lambda = 0$ and similar behaviors for $\lambda \leq 1$. Instead, when PBE orbitals are used, larger differences between the Au_2 and twice the Au curves can be noted. These originate only partially from the fact that, in the case of PBE orbitals, the exact exchange contributions of Au_2 and twice Au are not much similar (they differ by 0.045 eV). Mostly they depend on the rather different GL2 correlation energies for the systems ($E_c^{\mathrm{GL2}}(\mathrm{Au_2}) - 2E_c^{GL2}(\mathrm{Au}) = -0.173eV$), which in turn trace back to the fact that the single particle energy gaps computed for Au_2 and Au are very different: 2.014 eV and 0.718 eV, respectively. Consequently, the atomization adiabatic connection integrand curve calculated with PBE orbitals is steeper than the Hartree-Fock-based one and therefore it yields significantly larger atomization XC energies. This results in a strong tendency of PBE-based ACII functionals to overbind the noble metal clusters.

D. Further analysis of the ACII's formulas

We have seen in Sec. III that SPL and LB formulas show overall better performances than ISI and revISI. As mentioned, the main difference between the two groups is that the former uses a three-parameters interpolation formula, while the latter make use of a fourth ingredient from the $\lambda \to \infty$ limit, i.e., the zero-point oscillation term $W'_\infty[\rho]$. The revISI formula also recovers the exact expansion at large λ to higher orders.[79] However, we have to keep in mind that the ingredients coming from the strong interaction limit are not computed exactly but approximated with the semilocal PC model. Comparison with the exact $W_\infty[\rho]$ and $W'_\infty[\rho]$ for light atoms[79,81] suggests that the PC approximation of the $W_\infty[\rho]$ term is more accurate than the one for $W'_\infty[\rho]$. Moreover, the parameters appearing in the PC model for $W_\infty[\rho]$ are all determined by the electrostatics of the PC cell, while in the case of $W'_\infty[\rho]$, the gradient expansion does not give a physical result, and one of the parameters has to be fixed in other ways, for example, by making the model exact for the He atom.[79]

Another important point to consider is that, as explained in Sec. IV C, we are using the ACII functionals with Hartree-Fock orbitals, which means that they are used as a correlation functional for the Hartree-Fock energy. In other words, the ACII correlation functionals are used here as an approximate resummation of the Møller-Plesset perturbation series: they recover the exact MP2 at weak coupling and perform much better than MP3 and MP4 for atomization energies (see Table II). Thus, a first question that needs to be addressed is whether the PC model used here to compute the infinite coupling strength functionals is accurate also for the Hartree-Fock adiabatic connection, in which the λ-dependent hamiltonian reads

$$\hat{H}^\lambda = \hat{T} + \hat{V}_{\mathrm{HF}} + \lambda\,(\hat{V}_{ee} - \hat{V}_{\mathrm{HF}}), \tag{12}$$

with $\hat{V}_{\mathrm{HF}}$ being the Hartree-Fock non local potential operator. This adiabatic connection is different from the DFT one, as the density is not fixed but changes with λ; the HF correlation energy is still given by a coupling-constant integration similar to the one of Eq. (2), as reviewed, for example, in Ref. 135. The perturbative expansion for small λ of Eq. (12) defines the MP series. When $\lambda \to \infty$, the problem defined by $\hat{H}^\lambda$ of Eq. (12) is also not the same as the one of the density-fixed adiabatic connection arising in DFT, but still it is defined in terms of the HF density. The results of this study suggest that the PC model can provide a decent approximation of the leading $\lambda \to \infty$ term in the HF adiabatic connection integrand, at least when dealing with isoelectronic energy differences. A careful study of the problem is the object of on-going work.

Keeping in mind that the information from $W'_\infty[\rho]$ is less accurate (and maybe less relevant in the HF context), it can be interesting to consider a variant of ISI and revISI, in which we replace $W'^{\mathrm{PC}}_\infty[\rho]$ with the curvature at $\lambda = 0$ (obtained from MP3) as an input ingredient. In this way, the modified AC integrand expressions recover the first three terms of Eq. (4) for small λ, and only the first term of Eq. (5) for large λ. However, the resulting XC approximations show several drawbacks. In fact, the results for atomization energies are significantly worse than for the original ISI and revISI functionals (the MAEs are 0.72 and 0.65 eV for Au clusters, 0.40 and 0.37 eV for Ag clusters, and 0.55 and 0.51 eV for binary clusters), despite they are close to the MP2 ones and better than the MP3 ones. More importantly, the modified ISI and revISI formulas, with the input ingredients for the Au and Ag clusters, result in adiabatic connection integrands that become imaginary at some $\lambda > 1$, with revISI breaking down at much larger λ values than ISI. This fact might be ascribed to the oscillatory behavior of the MP series, which gives a curvature that is too large, or to the lack of flexibility of the revISI and ISI formulas. This is further illustrated in the Appendix.

V. CONCLUSIONS AND PERSPECTIVES

We have assessed the performance of functionals based on the idea of interpolating between the weak- and the

strong-interaction limits, the global adiabatic-connection integrand (ACII functionals), for noble-metal clusters, analyzing and rationalizing different features of this approach. The study presented here extends a previous preliminary assessment on main group chemistry[82] and explores different interpolation formulas.

We have found that the ACII functionals, although not spectacularly accurate, are quite robust for the description of atomization energies, as their performance tends to be the same for different species and different cluster sizes, which is a positive feature. We should also stress that this good performance is achieved by using 100% of Hartree-Fock exchange and thus avoiding to rely on error cancellation between exchange and correlation. Rather, as clearly shown in Fig. 3, this is achieved by performing in a very similar way for the description of a cluster and its constituent atoms. On the other hand, the ACII functionals are found to be inaccurate for ionization energies, as they are not capable to describe differently charged states of the same system with the same accuracy, as shown in Fig. 4.

As in the case of main-group chemistry,[82] we have found that the ACII functionals perform much better when used with Hartree-Fock orbitals, which means that they are used as a correlation functional for the Hartree-Fock energy. In other words, the ACII correlation functionals are used here as an approximate resummation of the Møller-Plesset perturbation series: they recover the exact MP2 at weak coupling and perform much better than MP3 and MP4 for atomization energies (see Table II). Thus, a first question that needs to be addressed is whether the PC model used here to compute the infinite coupling strength functionals is accurate also for the Hartree-Fock adiabatic connection of Eq. (12), which is the object of a current investigation. The results of this study and of Ref. 82 suggest that the PC model can provide a decent approximation of the $\lambda \to \infty$ HF adiabatic connection integrand, at least when dealing with isoelectronic energy differences.

Another promising future direction is the development of ACII functionals in which the interpolation is done in each point of space, on energy densities.[87–89] These local interpolations are more amenable to construct size-consistent approximations but need energy densities all defined in the same gauge (one of the electrostatic potentials of the exchange-correlation hole seems so far to be the most suitable for this purpose[136]). In this framework, the simple PC model, which performs globally quite well, does not provide accurate approximations pointwise[89] and needs to be replaced with models based on integrals of the spherically averaged density,[91,92] which, in turn, needs a careful implementation, which is the focus of on-going efforts.[92] Finally, recent models for $\lambda = 1$ could be also used in this framework,[93] both locally and globally.

ACKNOWLEDGMENTS

Financial support was provided by the European Research Council under No. H2020/ERC Consolidator Grant corr-DFT (Grant No. 648932). We thank TURBOMOLE GmbH for providing the TURBOMOLE program package.

APPENDIX: ADIABATIC CONNECTION INTEGRAND INTERPOLATION FORMULAS

Several interpolation formulas have been developed to recover the weak- and strong-coupling limit behaviors of Eqs. (4) and (5). For the sake of simplicity, we will not specify in the following that the expressions of the AC integrand and of the XC correlation energy are (explicit or implicit) functionals of the density as well as each of their fundamental ingredients, W_0, W_0', W_0'', W_∞, and W_∞'.

Interaction Strength Interpolation (ISI) formula[75–77,82]

$$W_\lambda^{\mathrm{ISI}} = W_\infty + \frac{X}{\sqrt{1+\lambda Y}+Z}\,, \tag{A1}$$

with

$$X = \frac{xy^2}{z^2}\,,\ Y = \frac{x^2y^2}{z^4}\,,\ Z = \frac{xy^2}{z^3} - 1\,, \tag{A2}$$

$$x = -2W_0',\ y = W_\infty'\,,\ z = W_0 - W_\infty\,. \tag{A3}$$

After integration in Eq. (2), it gives

$$E_{xc}^{\mathrm{ISI}} = W_\infty + \frac{2X}{Y}\left[\sqrt{1+Y} - 1 - Z\ln\left(\frac{\sqrt{1+Y}+Z}{1+Z}\right)\right]\,. \tag{A4}$$

Revised ISI (revISI) formula[79]

$$W_\lambda^{\mathrm{revISI}} = W_\infty + \frac{b\left(2+c\lambda+2d\sqrt{1+c\lambda}\right)}{2\sqrt{1+c\lambda}\left(d+\sqrt{1+c\lambda}\right)^2}, \tag{A5}$$

where

$$b = -\frac{4W_0'(W_\infty')^2}{(W_0-W_\infty)^2}\,,\ c = \frac{2(W_0'W_\infty')^2}{(W_0-W_\infty)^4}\,,$$
$$d = -1 - \frac{4W_0'(W_\infty')^2}{(W_0-W_\infty)^3}\,. \tag{A6}$$

The corresponding XC functional is

$$E_{xc}^{\mathrm{revISI}} = W_\infty + \frac{b}{\sqrt{1+c}+d}\,. \tag{A7}$$

Seidl-Perdew-Levy (SPL) formula[83]

$$W_\lambda^{\mathrm{SPL}} = W_\infty + \frac{W_0 - W_\infty}{\sqrt{1+2\lambda\chi}}\,, \tag{A8}$$

with

$$\chi = \frac{W_0'}{W_\infty - W_0}\,. \tag{A9}$$

The SPL XC functional reads

$$E_{xc}^{\mathrm{SPL}} = (W_0 - W_\infty)\left[\frac{\sqrt{1+2\chi}-1-\chi}{\chi}\right] + W_0\,. \tag{A10}$$

Note that this functional does not make use on information on W_∞'.

Liu-Burke (LB) formula[84]

$$W_\lambda^{\mathrm{LB}} = W_\infty + \beta(y+y^4)\,, \tag{A11}$$

where

$$y = \frac{1}{\sqrt{1+\gamma\lambda}}\ ,\ \beta = \frac{W_0 - W_\infty}{2}\ ,\ \gamma = \frac{4W_0'}{5(W_\infty - W_0)}\ . \quad \text{(A12)}$$

Using Eq. (2), the LB XC functional is found to be

$$E_{xc}^{\mathrm{LB}} = 2\beta\left[\frac{1}{\gamma}\left(\sqrt{1+c} - \frac{1+c/2}{1+c}\right) - 1\right]\ . \quad \text{(A13)}$$

Also the LB functional does not use information on W_∞'.

Point-Charge-plus-continuum (PC) model

In all cases, the highly non-local functionals W_∞ and W_∞' (when used) are approximated by the semilocal PC model[76]

$$W_\infty \approx W_\infty^{\mathrm{PC}} = \int\left[A\rho(\mathbf{r}^{4/3}) + B\frac{|\nabla\rho(\mathbf{r})|^2}{\rho(\mathbf{r})^{4/3}}\right]d\mathbf{r}, \quad \text{(A14)}$$

$$W_\infty' \approx W_\infty'^{\,\mathrm{PC}} = \int\left[C\rho(\mathbf{r}^{3/2}) + D\frac{|\nabla\rho(\mathbf{r})|^2}{\rho(\mathbf{r})^{7/6}}\right]d\mathbf{r}\ , \quad \text{(A15)}$$

where $A = -9(4\pi/3)^{1/3}/10$, $B = 3[3/(4\pi)]^{1/3}/350$, $C = \sqrt{3\pi}/2$, $D = -0.028\,957$; note that other slightly different values are possible for the D parameter.[79]

1. ISI and revISI with the exact curvature

The ISI and revISI formulas have four parameters that need to be fixed by four equations. In the standard forms (see above), the four equations are obtained by imposing that W_λ^{ISI} recovers the first two terms of the weak-interacting limit expansion, Eq. (4), and the first two terms in the strongly interacting limit expansion, Eq. (5) for large λ. For the first time, we have explored an alternative choice that is to constrain ISI and revISI to recover the first three terms of Eq. (4) for small λ and only the first term of Eq. (5).

The structure of the interpolation formula is thus formally the same, but the parameters are given by

$$\begin{aligned} X &= -2(W_0 - W_\infty) + \frac{W_0''}{(W_0')^2}(W_0 - W_\infty)^2, \\ Y &= -2\frac{W_0''}{W_0'} + \frac{4W_0'}{(W_0 - W_\infty)}, \\ Z &= -3 + \frac{W_0''}{(W_0')^2}(W_0 - W_\infty), \end{aligned} \quad \text{(A16)}$$

for ISI, and

$$\begin{aligned} b &= -2(W_0 - W_\infty) + \frac{4W_0''(W_0 - W_\infty)^2}{3(W_0')^2}, \\ c &= -\frac{4W_0''}{3W_0'} + \frac{2W_0'}{(W_0 - W_\infty)}, \\ d &= -3 + \frac{4W_0''(W_0 - W_\infty)}{3(W_0')^2}, \end{aligned} \quad \text{(A17)}$$

for revISI.

However, as discussed in Sec. IV D, while in the standard ISI and revISI interpolation formulas, the parameters, $Y[\rho]$ and $c[\rho]$, which appear under square root, are given by the sum of squared quantities [see Eqs. (A2) and (A6)]; in these modified versions, this is not true and they can become negative. In the cases studied here, both parameters turn out to be always negative and smaller than one, meaning that there is, for each species, a critical lambda, λ_c, always larger than one, after which the function takes imaginary values. In particular, we found an average $\bar{\lambda}_c^{ISI} \approx 4$ with values spanning from 2.5 to 5.7, and an average $\bar{\lambda}_c^{revISI} \approx 180$ with values spanning from 6 to over 3×10^3. As a general trend, we thus see that the modified revISI appears to be more robust than the modified ISI in the sense that it becomes imaginary at significantly larger λ values.

[1] H. Schmidbaur, Gold Bull. **23**, 11 (1990).
[2] M.-C. Daniel and D. Astruc, Chem. Rev. **104**, 293 (2004).
[3] P. Pyykkö, Angew. Chem., Int. Ed. **43**, 4412 (2004).
[4] P. Schwerdtfeger and M. Lein, "Theoretical chemistry of gold–From atoms to molecules, clusters, surfaces and the solid state," in *Gold Chemistry: Applications and Future Directions in the Life Sciences*, edited by F. Mohr (Wiley-VCH, Oxford, 2009).
[5] P. Pyykkö, Inorg. Chim. Acta **358**, 4113 (2005), protagonists in chemistry–Hubert Schmidbaur.
[6] P. Pyykkö, Chem. Soc. Rev. **37**, 1967 (2008).
[7] V. W.-W. Yam and E. C.-C. Cheng, Chem. Soc. Rev. **37**, 1806 (2008).
[8] G. J. Hutchings, M. Brust, and H. Schmidbaur, Chem. Soc. Rev. **37**, 1759 (2008).
[9] S. Yamazoe, K. Koyasu, and T. Tsukuda, Acc. Chem. Res. **47**, 816 (2014).
[10] T. Ayako and H. Masatake, Chem. Lett. **43**, 380 (2014).
[11] *Gold Nanoparticles for Physics, Chemistry and Biology*, edited by C. Louis and O. Pluchery (World Scientific, Singapore, 2017).
[12] M. Haruta, Gold Bull. **37**, 27 (2004).
[13] T. Takei, T. Akita, I. Nakamura, T. Fujitani, M. Okumura, K. Okazaki, J. Huang, T. Ishida, and M. Haruta, *Advances in Catalysis* (Academic Press, 2012), pp. 1–126.
[14] T. Ishida, H. Koga, M. Okumura, and M. Haruta, Chem. Rec. **16**, 2278 (2016).
[15] A. Mathew and T. Pradeep, Part. Part. Syst. Charact. **31**, 1017 (2014).
[16] M. Pereiro, D. Baldomir, J. Botana, J. E. Arias, K. Warda, and L. Wojtczak, J. Appl. Phys. **103**, 07A315 (2008).
[17] S. M. Novikov, V. N. Popok, A. B. Evlyukhin, M. Hanif, P. Morgen, J. Fiutowski, J. Beermann, H.-G. Rubahn, and S. I. Bozhevolnyi, Langmuir **33**, 6062 (2017).
[18] I. Díez and R. H. A. Ras, "Few-atom silver clusters as fluorescent reporters," in *Advanced Fluorescence Reporters in Chemistry and Biology. II. Molecular Constructions, Polymers and Nanoparticles*, edited by A. P. Demchenko (Springer Berlin Heidelberg, Berlin, Heidelberg, 2010), pp. 307–332.
[19] M. Ganguly, J. Jana, A. Pal, and T. Pal, RSC Adv. **6**, 17683 (2016).
[20] T. M. Bernhardt, Int. J. Mass Spectrom. **243**, 1 (2005).
[21] L. D. Socaciu, J. Hagen, J. L. Roux, D. Popolan, T. M. Bernhardt, L. Wöste, and Štefan Vajda, J. Chem. Phys. **120**, 2078 (2004).
[22] T. Vosch, Y. Antoku, J.-C. Hsiang, C. I. Richards, J. I. Gonzalez, and R. M. Dickson, Proc. Natl. Acad. Sci. **104**, 12616 (2007).
[23] S. A. Khan, D. Senapati, T. Senapati, P. Bonifassi, Z. Fan, A. K. Singh, A. Neeley, G. Hill, and P. C. Ray, Chem. Phys. Lett. **512**, 92 (2011).
[24] E. C. Tyo and S. Vajda, Nat. Nanotechnol. **10**, 577–588 (2015).
[25] M. Yang, K. A. Jackson, and J. Jellinek, J. Chem. Phys. **125**, 144308 (2006).
[26] B. Yoon, P. Koskinen, B. Huber, O. Kostko, B. von Issendorff, H. Häkkinen, M. Moseler, and U. Landman, ChemPhysChem **8**, 157 (2007).
[27] N. Shao, W. Huang, Y. Gao, L.-M. Wang, X. Li, L.-S. Wang, and X. C. Zeng, J. Am. Chem. Soc. **132**, 6596 (2010).
[28] X. Xing, B. Yoon, U. Landman, and J. H. Parks, Phys. Rev. B **74**, 165423 (2006).
[29] H. Hakkinen, Chem. Soc. Rev. **37**, 1847 (2008).
[30] L.-M. Wang and L.-S. Wang, Nanoscale **4**, 4038 (2012).
[31] Y. Dong and M. Springborg, J. Phys. Chem. C **111**, 12528 (2007).
[32] A. Tanwar, E. Fabiano, P. E. Trevisanutto, L. Chiodo, and F. Della Sala, Eur. Phys. J. B **86**, 161 (2013).
[33] E. Fabiano, L. A. Constantin, and F. D. Sala, J. Chem. Phys. **134**, 194112 (2011).
[34] E. Fabiano, M. Piacenza, and F. Della Sala, Phys. Chem. Chem. Phys. **11**, 9160 (2009).

[35]M. V. Popa, Int. J. Comput. Theor. Chem. **3**, 36 (2015).
[36]R. K. Hailstone and J. Tan, J. Imaging Sci. Technol. **46**, 81 (2002).
[37]M. L. McKee and A. Samokhvalov, J. Phys. Chem. A **121**, 5018 (2017).
[38]K. Duanmu and D. G. Truhlar, J. Phys. Chem. C **119**, 9617 (2015).
[39]P. Weis, T. Bierweiler, S. Gilb, and M. M. Kappes, Chem. Phys. Lett. **355**, 355 (2002).
[40]D. Schooss, P. Weis, O. Hampe, and M. M. Kappes, Philos. Trans. R. Soc., A **368**, 1211 (2010).
[41]K. J. Taylor, C. L. Pettiette-Hall, O. Cheshnovsky, and R. E. Smalley, J. Chem. Phys. **96**, 3319 (1992).
[42]B. F. G. Johnson and S. McIndoe, Coord. Chem. Rev. **200-202**, 901 (2000).
[43]*Atomic Clusters: From Gas Phase to Deposited*, edited by D. P. Wooddruff (Elsevier, Amsterdam, 2007).
[44]A. Fielicke, A. Kirilyuk, C. Ratsch, J. Behler, M. Scheffler, G. von Helden, and G. Meijer, Phys. Rev. Lett. **93**, 023401 (2004).
[45]M. Haertelt, V. J. F. Lapoutre, J. M. Bakker, B. Redlich, D. J. Harding, A. Fielicke, and G. Meijer, J. Phys. Chem. Lett. **2**, 1720 (2011).
[46]C. S. Creaser, J. R. Griffiths, C. J. Bramwell, S. Noreen, C. A. Hill, and C. L. P. Thomas, Analyst **129**, 984 (2004).
[47]F. Lanucara, S. W. Holman, C. J. Gray, and E. C. Eyers, Nat. Chem. **6**, 281 (2014).
[48]N. S. Khetrapal, S. S. Bulusu, and X. C. Zeng, J. Phys. Chem. A **121**, 2466 (2017).
[49]F. Furche, R. Ahlrichs, P. Weis, C. Jacob, S. Gilb, T. Bierweiler, and M. M. Kappes, J. Chem. Phys. **117**, 6982 (2002).
[50]M. P. Johansson, A. Lechtken, D. Schooss, M. M. Kappes, and F. Furche, Phys. Rev. A **77**, 053202 (2008).
[51]A. Lechtken, C. Neiss, M. M. Kappes, and D. Schooss, Phys. Chem. Chem. Phys. **11**, 4344 (2009).
[52]M. N. Blom, D. Schooss, J. Stairs, and M. M. Kappes, J. Chem. Phys. **124**, 244308 (2006).
[53]M. Reiher, Chimia Int. J. Chem. **63**, 140 (2009).
[54]*Recent Advances in Multireference Methods*, edited by K. Hirao (World Scientific, Singapore, 1999).
[55]B. O. Roos, in *Theory and Applications of Computational Chemistry: The First Forty Years*, edited by C. E. Dykstra, G. Frenking, K. S. Kim, and G.E. Scuseria (Elsevier, Amsterdam, 2005).
[56]C. Møller and M. S. Plesset, Phys. Rev. **46**, 618 (1934).
[57]D. Cremer, Wiley Interdiscip. Rev.: Comput. Mol. Sci. **1**, 509 (2011).
[58]C. D. Sherrill and H. F. Schaefer III, *Advances in Quantum Chemistry* (Academic Press, 1999), pp. 143–269.
[59]I. Shavitt, Mol. Phys. **94**, 3 (1998).
[60]T. D. Crawford and H. F. Schaefer III, in *Reviews in Computational Chemistry*, edited by K. B. Lipkowitz and D. B. Boyd (Wiley-VCH, New York, 2000).
[61]J. Čížek, Theor. Chim. Acta **80**, 91 (1991).
[62]W. Kohn and L. J. Sham, Phys. Rev. **140**, A1133 (1965).
[63]E. K. U. Gross and R. M. Dreizler, *Density Functional Theory* (Springer Science+Business Media, New York, 1995).
[64]F. M. Bickelhaupt and E. J. Baerends, "Kohn-Sham density functional theory: Predicting and understanding chemistry," in *Reviews in Computational Chemistry* (John Wiley & Sons, Inc., 2007), pp. 1–86.
[65]V. N. Staroverov and G. E. Scuseria, in *Theory and Applications of Computational Chemistry: The First Forty Years*, edited by C. E. Dykstra, G. Frenking, K. S. Kim, and G. E. Scuseria (Elsevier, Amsterdam, 2005).
[66]F. Della Sala, E. Fabiano, and L. A. Constantin, Int. J. Quantum Chem. **116**, 1641 (2016).
[67]M. Chen, J. E. Dyer, K. Li, and D. A. Dixon, J. Phys. Chem. A **117**, 8298 (2013).
[68]G. Zanti and D. Peeters, Theor. Chem. Acc. **132**, 1300 (2012).
[69]H. Baek, J. Moon, and J. Kim, J. Phys. Chem. A **121**, 2410 (2017).
[70]K. Sharkas, J. Toulouse, and A. Savin, J. Chem. Phys. **134**, 064113 (2011).
[71]A. D. Becke, J. Chem. Phys. **98**, 1372 (1993).
[72]M. Ernzerhof, Chem. Phys. Lett. **263**, 499 (1996).
[73]J. P. Perdew, M. Ernzerhof, and K. Burke, J. Chem. Phys. **105**, 9982 (1996).
[74]E. Fabiano, L. A. Constantin, P. Cortona, and F. Della Sala, J. Chem. Theory Comput. **11**, 122 (2015).
[75]M. Seidl, J. P. Perdew, and S. Kurth, Phys. Rev. Lett. **84**, 5070 (2000).
[76]M. Seidl, J. P. Perdew, and S. Kurth, Phys. Rev. A **62**, 012502 (2000).
[77]M. Seidl, J. P. Perdew, and S. Kurth, Phys. Rev. A **72**, 029904(E) (2005).
[78]A. Görling and M. Levy, Phys. Rev. A **50**, 196 (1994).
[79]P. Gori-Giorgi, G. Vignale, and M. Seidl, J. Chem. Theory Comput. **5**, 743 (2009).
[80]M. Seidl, Phys. Rev. A **60**, 4387 (1999).
[81]M. Seidl, P. Gori-Giorgi, and A. Savin, Phys. Rev. A **75**, 042511 (2007).
[82]E. Fabiano, P. Gori-Giorgi, M. Seidl, and F. Della Sala, J. Chem. Theory Comput. **12**, 4885 (2016).
[83]M. Seidl, J. P. Perdew, and M. Levy, Phys. Rev. A **59**, 51 (1999).
[84]Z. F. Liu and K. Burke, Phys. Rev. A **79**, 064503 (2009).
[85]P. Gori-Giorgi and A. Savin, J. Phys.: Conf. Ser. **117**, 012017 (2008).
[86]A. Savin, Chem. Phys. **356**, 91 (2009).
[87]Y. Zhou, H. Bahmann, and M. Ernzerhof, J. Chem. Phys. **143**, 124103 (2015).
[88]S. Vuckovic, T. J. P. Irons, A. Savin, A. M. Teale, and P. Gori-Giorgi, J. Chem. Theory Comput. **12**, 2598–2610 (2016).
[89]S. Vuckovic, T. J. P. Irons, L. O. Wagner, A. M. Teale, and P. Gori-Giorgi, Phys. Chem. Chem. Phys. **19**, 6169 (2017).
[90]A. Mirtschink, M. Seidl, and P. Gori-Giorgi, J. Chem. Theory Comput. **8**, 3097 (2012).
[91]L. O. Wagner and P. Gori-Giorgi, Phys. Rev. A **90**, 052512 (2014).
[92]H. Bahmann, Y. Zhou, and M. Ernzerhof, J. Chem. Phys. **145**, 124104 (2016).
[93]S. Vuckovic and P. Gori-Giorgi, J. Phys. Chem. Lett. **8**, 2799 (2017).
[94]J. P. Perdew, K. Burke, and M. Ernzerhof, Phys. Rev. Lett. **77**, 3865 (1996).
[95]C. Adamo and V. Barone, J. Chem. Phys. **110**, 6158 (1999).
[96]S. Grimme, J. Chem. Phys. **124**, 034108 (2006).
[97]G. D. Purvis III and R. J. Bartlett, J. Chem. Phys. **76**, 1910 (1982).
[98]J. A. Pople, M. Head-Gordon, and K. Raghavachari, J. Chem. Phys. **87**, 5968 (1987).
[99]G. E. Scuseria, C. L. Janssen, and H. F. Schaefer III, J. Chem. Phys. **89**, 7382 (1988).
[100]K. Raghavachari, G. W. Trucks, J. A. Pople, and M. Head-Gordon, Chem. Phys. Lett. **157**, 479 (1989).
[101]V. Bonačić-Koutecký, J. Burda, R. Mitrić, M. Ge, G. Zampella, and P. Fantucci, J. Chem. Phys. **117**, 3120 (2002).
[102]J. P. Perdew, A. Ruzsinszky, G. I. Csonka, L. A. Constantin, and J. Sun, Phys. Rev. Lett. **103**, 026403 (2009).
[103]F. Weigend and R. Ahlrichs, Phys. Chem. Chem. Phys. **7**, 3297 (2005).
[104]J. C. Fabbi, J. D. Langenberg, Q. D. Costello, M. D. Morse, and L. Karlsson, J. Chem. Phys. **115**, 7543 (2001).
[105]B. Chan and W.-L. Yim, J. Chem. Theory Comput. **9**, 1964 (2013).
[106]M. N. Huda and A. K. Ray, Eur. Phys. J. D **22**, 217 (2003).
[107]Y.-K. Shi, Z. H. Li, and K.-N. Fan, J. Phys. Chem. A **114**, 10297 (2010).
[108]R. Wesendrup, T. Hunt, and P. Schwerdtfeger, J. Chem. Phys. **112**, 9356 (2000).
[109]J. Yoon, K. S. Kim, and K. K. Baeck, J. Chem. Phys. **112**, 9335 (2000).
[110]M.-J. Huang and J. D. Watts, Phys. Chem. Chem. Phys. **14**, 6849 (2012).
[111]C. L. Janssen and I. M. Nielsen, Chem. Phys. Lett. **290**, 423 (1998).
[112]M. L. Leininger, I. M. Nielsen, T. Crawford, and C. L. Janssen, Chem. Phys. Lett. **328**, 431 (2000).
[113]W. Jiang, N. J. DeYonker, and A. K. Wilson, J. Chem. Theory Comput. **8**, 460 (2012).
[114]H.-P. Loock, L. M. Beaty, and B. Simard, Phys. Rev. A **59**, 873 (2009).
[115]H. Häkkinen, B. Yoon, U. Landman, X. Li, H.-J. Zhai, and L.-S. Wang, J. Phys. Chem. A **107**, 6168 (2003).
[116]K. Balasubramanian and P. Y. Feng, Chem. Phys. Lett. **159**, 452 (1989).
[117]K. P. Huber and G. Herzberg, *Molecular Spectra and Molecular Structure* (Springer, 1979).
[118]V. Beutel, H.-G. Kramer, G. Bhale, M. Kuhn, K. Weyers, and W. Demtroder, J. Chem. Phys. **98**, 2699 (1993).
[119]V. A. Spasov, T. H. Lee, J. P. Maberry, and K. Ervin, J. Chem. Phys. **110**, 5208 (1999).
[120]H. M. Lee, M. Ge, B. R. Sahu, P. Tarakeshwar, and K. S. Kim, J. Phys. Chem. B **107**, 9994 (2003).
[121]L. A. Constantin, E. Fabiano, and F. Della Sala, J. Chem. Theory Comput. **9**, 2256 (2013).
[122]L. A. Constantin, E. Fabiano, and F. D. Sala, Phys. Rev. B **86**, 035130 (2012).
[123]L. A. Constantin, E. Fabiano, and F. Della Sala, Phys. Rev. B **88**, 125112 (2013).
[124]See http://www.turbomole.com for TURBOMOLE, TURBOMOLE, V7.0; TURBOMOLE GmbH: Karlsruhe, Germany, 2011 (accessed March, 2017).
[125]F. Furche, R. Ahlrichs, C. Hättig, W. Klopper, M. Sierka, and F. Weigend, Wiley Interdiscip. Rev.: Comput. Mol. Sci. **4**, 91 (2014).
[126]J. G. Hill and K. A. Peterson, J. Chem. Theory Comput. **8**, 518 (2012).

[127]D. Figgen, G. Rauhut, M. Dolg, and H. Stoll, Chem. Phys. **311**, 227 (2005), relativistic effects in heavy-element chemistry and physics, in memoriam Bernd A. Hess (1954–2004).
[128]J. van der Tol, D. Jia, Y. Li, V. Chernyy, J. M. Bakker, M. T. Nguyen, P. Lievens, and E. Janssens, Phys. Chem. Chem. Phys. **19**, 19360 (2017).
[129]S. Krückeberg, G. Dietrich, K. Lützenkirchen, L. Schweikhard, C. Walther, and J. Ziegler, Int. J. Mass Spectrom. Ion Processes **155**, 141 (1996).
[130]M. Mantina, R. Valero, and D. G. Truhlar, J. Chem. Phys. **131**, 064706 (2009).
[131]F. Colonna and A. Savin, J. Chem. Phys. **110**, 2828 (1999).
[132]A. M. Teale, S. Coriani, and T. Helgaker, J. Chem. Phys. **130**, 104111 (2009).
[133]A. M. Teale, S. Coriani, and T. Helgaker, J. Chem. Phys. **132**, 164115 (2010).
[134]S. Vuckovic, P. Gori-Giorgi, F. Della Sala, and E. Fabiano, e-print arXiv:1802.02144 [physics.chem-ph].
[135]K. Pernal, Int. J. Quantum Chem. **118**, e25462 (2018).
[136]S. Vuckovic, M. Levy, and P. Gori-Giorgi, J. Chem. Phys. **147**, 214107 (2017).